

Loss of ductility due to the decarburization and Mn depletion of a coarse-grained TWIP steel

Fernando de las Cuevas^{a,b,✉}, Javier Gil Sevillano^c

^a UPNA (Universidad Pública de Navarra), Campus de Arrosadia Dpto. de Física, 31006 Pamplona, España

^b Siemens Gamesa Renewable Energy Innovation & Technology, S.L., Avda. Ciudad de la Innovación 2, 31621 Sarriguren, Navarra, España

^c CEIT y TECNUN (Universidad de Navarra), C/ M. Lardizábal 15, 20018 San Sebastián, España

✉ Corresponding Author: fernando.delascuevas@unavarra.es

Submitted: 24 May 2017; Accepted: 26 July 2017; Available On-line: 18 December 2017

ABSTRACT: A clear transition in the tensile ductility behavior has been observed for grain sizes D in the range of $15\ \mu\text{m} - 20\ \mu\text{m}$ ($1.50\ \mu\text{m} \leq D < 50\ \mu\text{m}$) in a 22% Mn, 0.6% C (in mass %) TWIP steel. This behavior is a combination of the intrinsic effect of grain size D on strength and work hardening rate of the material, with an extrinsic effect, superficial decarburization and Mn depletion processes occurred during annealing treatments at $T \geq 1000\ \text{°C}$. In the present work, this extrinsic effect happened in TWIP steel has been studied in depth. GDOES (Glow Discharge Optical Emission Spectrometry) analyses have been carried out in order to study quantitatively the C and Mn concentration profiles. The depth of surface decarburization has been modeled by using Birks-Jackson theory. Two micro-constituents have been observed via Ferritoscope into decarburized volume: α' -martensite and γ -austenite. The ductility of coarse-grained TWIP steel, subjected for high annealing temperatures and long annealing times, declines as a consequence of the formation of α' -martensite and less stable γ -austenite with lower stacking fault energy, SFE, due to the Mn depletion in the decarburized volume.

KEYWORDS: Decarburization; Stacking fault energy (SFE); Twinning; TWIP steel; α' - martensite; γ – austenite

Citation/Citar como: de las Cuevas, F.; Gil Sevillano, J. (2017) “Loss of ductility due to the decarburization and Mn depletion of a coarse-grained twip steel”. *Rev. Metal.* 53 (4):e109. <http://dx.doi.org/10.3989/revmetalm.109>

RESUMEN: *Pérdida de ductilidad debido a la descarburación y pérdida de Mn de un acero TWIP de tamaño de grano grosero.* Se ha observado una clara transición de la ductilidad a tracción con el tamaño de grano D del orden $15\ \mu\text{m} - 20\ \mu\text{m}$ ($1,50\ \mu\text{m} \leq D < 50\ \mu\text{m}$) en un acero TWIP, 22% de Mn, 0,6% de C (% en masa). Este comportamiento es una combinación de un efecto intrínseco del tamaño de grano D en la resistencia y el endurecimiento por deformación del material, con un efecto extrínseco, proceso de descarburación superficial y pérdida de Mn ocurrido durante los tratamientos de recocido a $T \geq 1000\ \text{°C}$. En el presente trabajo se ha estudiado en profundidad este efecto extrínseco sucedido en el acero TWIP. Se han realizado análisis por GDOES (Espectroscopia Óptica de Descarga Luminiscente) para estudiar cuantitativamente los perfiles de concentración de C y Mn. La profundidad de descarburación superficial se ha modelizado usando la teoría de Birks-Jackson. Se ha observado vía ferritoscopio que, en el volumen descarburizado, coexisten dos microconstituyentes: α' -martensita y γ -austenita. La ductilidad del acero TWIP de tamaño de grano grosero, sometido a altas temperaturas y largos tiempos de recocido, disminuye como consecuencia de la formación de α' -martensita y γ -austenita menos estable con menor energía de defectos de apilamiento, EDA, debido a la pérdida de Mn en el volumen descarburizado.

PALABRAS CLAVE: Acero TWIP; Descarburación; Energía de defectos de apilamiento (EDA); Maclaje; α' - martensita; γ – austenita

ORCID ID: Fernando de las Cuevas (<http://orcid.org/0000-0002-2344-7353>); Javier Gil Sevillano (<http://orcid.org/0000-0002-1716-8200>)

Copyright: © 2017 CSIC. This is an open-access article distributed under the terms of the Creative Commons Attribution License (CC BY) Spain 3.0.

1. INTRODUCTION

Over last years, the twinning - induced plasticity Fe-Mn-C (TWIP) steels have been the center of intensive research works due to their outstanding tensile strength – ductility combination which arises from the formation of extensive mechanical twinning under mechanical loads (Frommeyer *et al.*, 2000; Cornette *et al.*, 2005; Scott *et al.*, 2006; Bouaziz *et al.*, 2008; Bouaziz *et al.*, 2011; Galán *et al.*, 2012; Gil Sevillano and De las Cuevas., 2012; Chen *et al.*, 2013; De las Cuevas *et al.*, 2014; Ghasri-Khouzani and McDermid, 2015; Pierce *et al.*, 2015).

The protruding mechanical properties of austenitic Fe-Mn-C steels were originally noticed and exploited by Sir Hadfield (1883) which adopted the name of Hadfield steels. Regrettably, the high carbon degrees (>1 wt.%) for thin sheet applications lead to carbide precipitation and, consequently, Hadfield steels have very restricted weldability and production processes. Besides, the relatively low Mn content (~ 15%) promotes strain induced martensitic transformation (SIMT) γ -austenite \rightarrow α' -martensite. By adjusting the chemical composition through an increase in the manganese and controlling the carbon concentration, the austenitic structure is preserved; the emergence of α' -martensite is inhibited and can lead to outstanding mechanical properties by (TWIP) effect (Grässel *et al.*, 1997; Frommeyer and Grässel, 1998; Grässel *et al.*, 2000). It is widely recognized that the TWIP effect occurs in a stable austenite rather than multiple martensitic transformations (γ -FCC \rightarrow ϵ -HCP \rightarrow α' -BCC) where the Gibbs free energy $\Delta G_{\gamma \rightarrow \epsilon}$ of the martensitic transformation is positive (around of 110 – 250 J·mol⁻¹) and the stacking fault energy (SFE) in the austenite is comparatively low, approximately 25 mJ·m⁻² (Frommeyer *et al.*, 2000). More recent literature on this point, Pierce *et al.* (2014) has shed more light on detailed aspects of the deformation mechanism, phase stability and SFE.

Fe-Mn-C austenitic steels can experience premature fracture depending on different microstructural conditions. On the one hand, premature fracture is promoted due to stress concentrations at the tips of ϵ -HCP martensite plates, Sipos *et al.* (1976), and in the interaction regions between annealing twin boundaries and ϵ -HCP martensite, Koyama *et al.* (2012a). On the other hand, premature fracture also takes place as a consequence of the mechanical twins interacting with: grain boundaries, Ankem *et al.* (1999); at cementite particles, Goldberg *et al.* (1992); in Mn-enriched segregation regions at grain boundaries, Tomota *et al.* (1987). Other phenomena found enclose failure owing to stress corrosion cracking, Khalissi *et al.* (2011), decarburization process, Lin *et al.* (2002), and hydrogen embrittlement (De Cooman *et al.*, 2011; Koyama *et al.*, 2012b).

In a previous work developed by De las Cuevas *et al.* (2010a), a clear transition in the tensile ductility behavior in terms of the uniform elongation ϵ_u and the area reduction at fracture A (%) has been found for a grain size of the order of 15 μ m - 20 μ m ($1.50 \mu\text{m} \leq D < 50 \mu\text{m}$) in a 22% Mn, 0.6% C (mass %) TWIP steel in tensile tests performed at room temperature and 10^{-3} s^{-1} . Indeed, for obtaining larger grain sizes, longer annealing times at high temperatures, $T \geq 1000 \text{ }^\circ\text{C}$, are required, which imply more oxidation on the specimen's surface. In the present work, decarburization and Mn depletion processes occurred during annealing treatments at $T \geq 1000 \text{ }^\circ\text{C}$ in TWIP steel has been studied in depth.

Key factors of decarburization process are the surface reactions of metal alloys with the environment. In addition, the driving force for decarburization in steel involves the exposure to oxygen at elevated temperatures, which is a condition fulfilled by hot working and heat treatments in air. Consequently, the reactants and products progressively disturb or modify the near-surface compositions, structures, and properties involving the removal of carbon (Birks *et al.*, 2006). The resulting near-surface compositional gradients can promote diffusion of elements from the alloy interior, including both bulk and grain boundary diffusion paths. This mass transfer leads to microstructural and property gradients (Birks *et al.*, 2006). This behavior has an undesirable effect on the properties of the alloy surface, lowering of strength and fatigue life of the material, and sophisticated process engineering is applied to inhibit or control the surface reactions (Birks *et al.*, 2006).

2. EXPERIMENTAL TECHNIQUE

2.1. Recrystallization conditions and grain growth

Hot rolled, laboratory-cast specimens of TWIP steel with 22% Mn and 0.6% C (mass %) were cold rolled. Next they were subjected to different annealing treatments in a salt bath furnace to obtain different equiaxed grain sizes after complete recrystallization and grain growth in the interval of $1.50 \mu\text{m} \leq D < 50 \mu\text{m}$. The samples were analyzed using a Philips XL30 SEM microscope equipped with a TSL module for automatic EBSD acquisition. The grain sizes of the specimens were resolved as the mean linear intercept using OIM-EBSD images. Further experimental details are reported (De las Cuevas *et al.*, 2010b).

2.2. Tensile tests

The tensile tests were carried out in an Instron machine at constant displacement rate at an initial strain rate of 10^{-3} s^{-1} . The sheet specimens comply with the standard ASTM E 8M-04 (sub-size, 6 mm

of wide, 32 mm of gauge length): In order to get such geometry, the specimens were machined by electrical discharge machining (EDM) after subjecting TWIP steel sheets to the different annealing treatments (de las Cuevas *et al.*, 2010a). The number of tensile tests was doubled for each grain size and good reproducibility of the experiments was obtained. The tensile strain was measured with a clip extensometer of 20 mm initial control length capable of 100% maximum elongation measurement. The area reduction at fracture, $A\%$, was measured from the separation of marks initially engraved at 25 mm of the gauge length.

2.3. Decarburation conditions

The effect of surface decarburization on TWIP steel performances was investigated in the interval of 300 s – 1100 s at 1000 °C and 1200 °C. After hot and cold rolling TWIP steel was annealed under N_2 fluxing (O_2 about 4-5%) at the soaking temperature of 1000 °C and 1200 °C for 300 s and 1100 s. These annealing treatments are required for getting coarse grain sizes of the order of 40 μm - 50 μm in the TWIP steel (De las Cuevas *et al.*, 2010b). A conventional medium-carbon C45 steel sample was used, as a reference, to compare the decarburization behaviour of TWIP steel at both temperatures. The compositions of both steels are presented in Table 1. All the strip samples of C45 steel (hot rolled state) were mechanically polished (about 1 mm was removed for each surface) to remove completely the scale layer and also the previous decarburized layer. After these operations, the samples were annealed at same conditions subjected by TWIP steel. For TWIP steel, the strip samples microstructures were analyzed under OM by means of the color etching Klemm's II. In the case of C45 steel, Nital (5% HNO_3) etching was used for revealing the microstructures. For both steels, the decarburization depth was evaluated metallographically since two different zones were denoted with different etching behaviour when moving from surface towards the bulk.

2.4. Ferritoscope and GDOES

Ferritoscope technique has been used in order to detect the presence of α' -martensite (BCC) in the microstructure close to the strip surface. The tests

TABLE 1. Chemical composition of TWIP and C45 steels

Material	Chemical composition (% In mass)						
	Fe	C	Mn	Si	N	S	P
C45 STEEL	BAL.	0.46	0.65	0.40	-	-	-
TWIP STEEL	BAL.	0.59	22.30	0.22	-	-	-

were performed using the FERITSCOPE FMP30, Fischer Technology, with the help of a measurement probe FGAB1.3 -Fe of the measurement range 0.1 - 80% Fe. The thickness of the test samples employed was 6 mm.

Glow discharge optical emission spectroscopy (GDOES) has been used for the characterization of the surfaces after annealing treatments at $T \geq 1000$ °C. For this work, a JY 5000 GDOES instrument was used in order to quantify C and Mn concentration due to its capacity to carry out elemental depth profiling with a refined spatial resolution from the surface to sub-surface of TWIP steel. The instrument was fitted with a standard 4 mm glow discharge source with both a polychromator and a monochromator. The optical path of the spectrometer was purged with nitrogen. The emission signals were obtained by selecting optimal operating conditions. The glow discharge source was controlled at a constant pressure of 450 Pa of Ar. Spectral emission lines were measured simultaneously with acquisition rate of one point per 1 s.

3. RESULTS

3.1. Quasi static tensile tests at room temperature: $10^{-3} s^{-1}$

In a previous research work carried out by De las Cuevas *et al.* (2010a), in order to study the grain size dependence on the tensile properties of TWIP steels, tensile tests at $10^{-3} s^{-1}$ were performed at room temperature. Figure 1 depicts the yield stress, σ_y , and the maximum uniform true stress, σ_u , as a function of grain size, D , which shows the expected trend for steels. Figure 2 shows the maximum uniform plastic strain, (ϵ_u), and the reduction of area at fracture, $A\%$ (with initial length, $l_0 = 25$ mm), as a function of grain size for the TWIP steel with composition 22% Mn, 0.6% C. It is worth noting that a clear transition in the tensile ductility behavior at grain size of the order of 15 μm - 20 μm is observed (see Fig. 2).

3.2. Decarburation at $T \geq 1000$ °C

In Fig. 3 the microstructures of the sub-surfaces of TWIP steel after annealing treatments 1000 °C - 300 s and 1200 °C - 1100 s are presented. Color etching Klemm's II was used for revealing the microstructures. The effect of the decarburization is quite clear in TWIP steel and typically two different zones are observed when moving from surface towards the bulk (different etching behavior). In addition, a large amount of α' -martensite has been detected in the sub-surfaces of both microstructures just after annealing at 1000 °C - 300 s and 1200 °C - 1100 s. It was confirmed by its magnetic behavior revealed by means of ferritoscope technique. This corroborates that the austenitic phase is destabilized

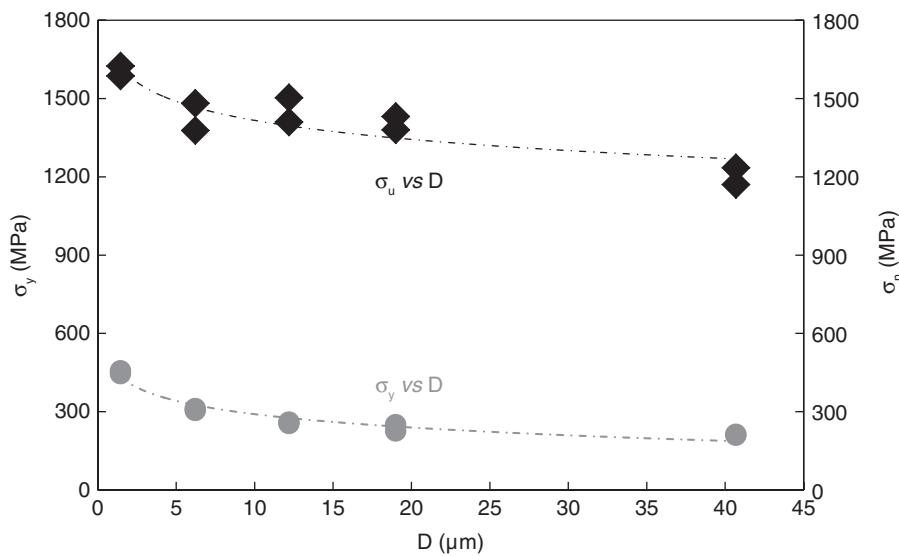


FIGURE 1. Yield stress at 0.2% plastic strain, (σ_y), and flow stress at the maximum uniform strain, (σ_u), as a function of grain size (D) for the TWIP steel with composition 22% Mn, 0.6% C. Duplicated tensile tests at room temperature and 10^{-3} s^{-1} .

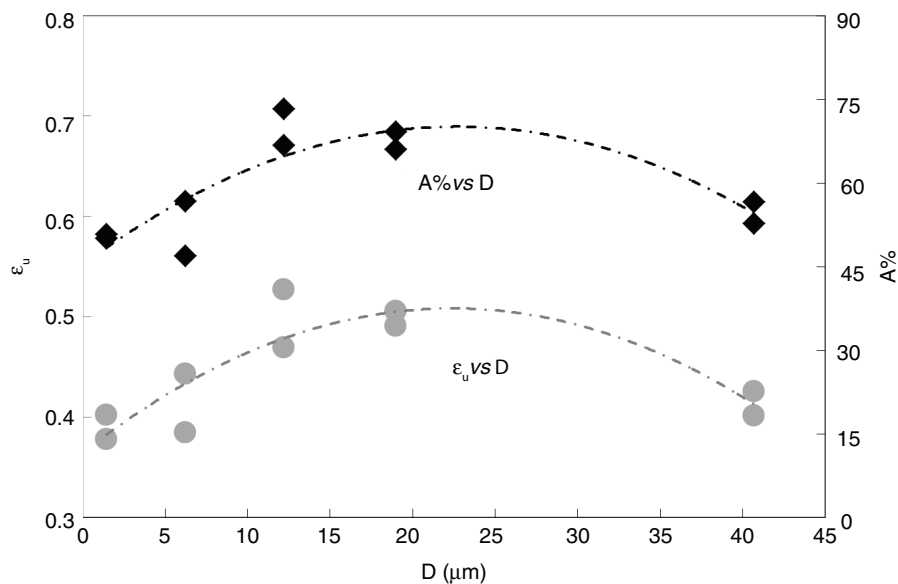


FIGURE 2. Maximum uniform plastic strain, (ϵ_u), and reduction of area at fracture, $A\%$, as a function of grain size (D) for the TWIP steel with composition 22% Mn, 0.6% C. Duplicated tensile tests at room temperature and 10^{-3} s^{-1} .

and the microstructure is a mixture of two microconstituents: γ -austenite and α -martensite. The decarburation depths, d_{exp} , estimated metallographically for TWIP steel were: $d_{exp}(\text{TWIP: } 1000 \text{ }^\circ\text{C} - 300 \text{ s}) = 115 \pm 10 \text{ } \mu\text{m}$ and $d_{exp}(\text{TWIP: } 1200 \text{ }^\circ\text{C} - 1100 \text{ s}) = 435 \pm 14 \text{ } \mu\text{m}$.

Figure 4a shows the microstructure of C45 steel before annealing (as hot rolled condition). Nital (5% HNO_3) etching was used for revealing the microstructures in all cases for this steel. The microstructure is the typical mixture of α -Ferrite (revealed as bright regions) and Pearlite (revealed as dark regions). In Fig. 4 (b and c) microstructures of C45 steel samples

after annealing treatments at $1000 \text{ }^\circ\text{C} - 300 \text{ s}$ and $1200 \text{ }^\circ\text{C} - 1100 \text{ s}$ are depicted for the sake of comparison with the TWIP steel. In both cases (Fig. 4b and 4c) two different zones can be found denoted with different etching behaviour when moving from surface towards the bulk. The outer zones of the sub-surfaces correspond to a majority α -Ferrite and the bulk represents the mixture of α -Ferrite and Pearlite. The large amount of α -Ferrite in the outer zones of the sub-surfaces indicates the intense of decarburation of C45 steel. The decarburation depths for C45 steel were: $d_{exp}(\text{C45: } 1000 \text{ }^\circ\text{C} - 300 \text{ s}) = 50 \pm 7 \text{ } \mu\text{m}$ and $d_{exp}(\text{C45: } 1200 \text{ }^\circ\text{C} - 1100 \text{ s}) = 310 \pm 12 \text{ } \mu\text{m}$.

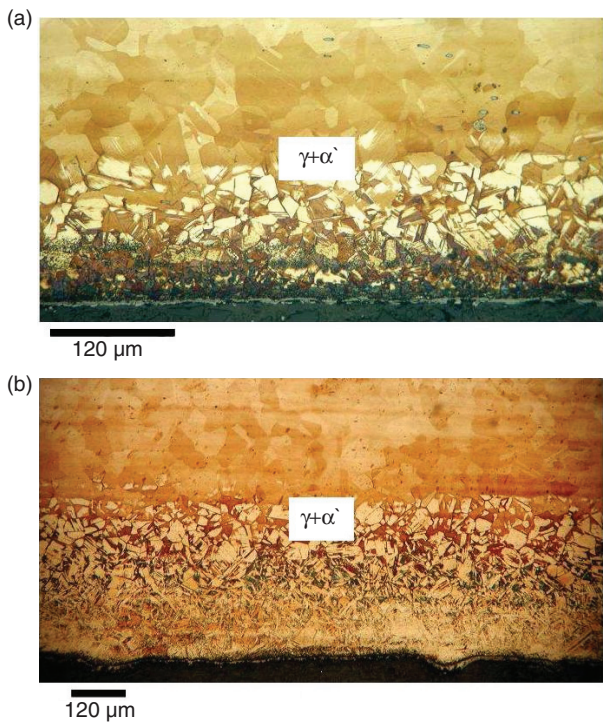


FIGURE 3. Sub-surface of TWIP steel with composition 22% Mn, 0.6% C after two different annealing treatments, color etching Klemm's II: (a) 1000 °C - 300 s and (b) 1200 °C - 1100 s. The bottom of each picture corresponds to mixed phases γ -austenite + α' -martensite.

In Fig. 5 the decarburization depth of TWIP steel is compared with the C45 medium carbon steel. As it can be seen, the decarburization depth of TWIP steel is larger than C45 medium carbon steel in the range of soaking time explored 300 s – 1100 s.

In TWIP steels, the application of the GDOES technique allows obtaining the C and Mn concentration profiles as the one shown in Fig. 6 for 1200 °C – 1100 s. Both C and Mn contents drop in the sub-surface zone during the annealing treatments at 1200 °C. The depth of Mn depleted zone (typically < 80 μm) is significantly lower than C decarburized layer (< 420 μm).

4. DISCUSSION

4.1. Modelling of the decarburization depth

For the modelling purposes, the decarburization is assumed to be a surface effect that only involves diffusion of carbon within the steel, i.e., the carbon depletion only occurs in the surface layer and the inner zone of the specimen maintains the original carbon composition C_0 , and then the problem may be treated for the case of a semi-infinite slab. The iron surface layer is assumed to be continuously removed by a simultaneous scaling reaction. The solution can also be simplified assuming the carbon diffusion coefficient is independent of the composition and

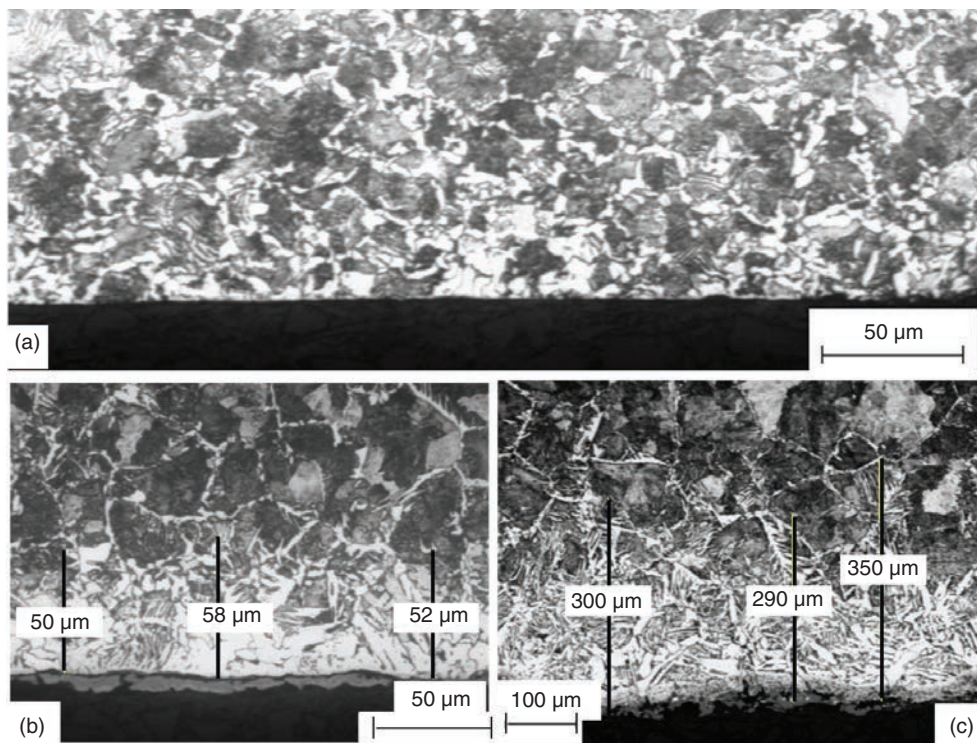


FIGURE 4. Sub-surface of C45 steel: (a) C45 strip surface structure before annealing (as hot rolled), after two different annealing treatments, (b) 1000 °C - 300 s and (c) 1200 °C - 1100 s.

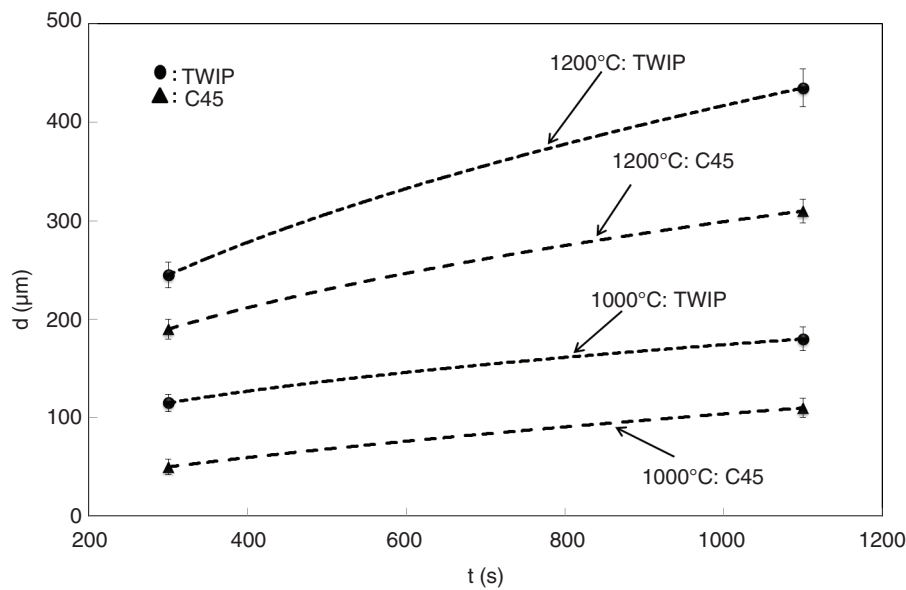


FIGURE 5. Decarburization depth as a function of annealing time in the interval 300 s -1100 s at 1000 °C and 1200 °C for both, TWIP and C45 steels.

grain boundary diffusion becomes negligible, which appears to be reasonable for coarse grained material. Then, the diffusion of carbon in the γ -austenite can be found by solving the Fick's second law, see Eq. (1) (Fick, 1855).

$$\frac{C}{C_0} = \text{erf}\left(\frac{x}{2\sqrt{D_c \cdot t}}\right) \quad (1)$$

Where C represents the concentration of an element at time t . C_0 is the concentration of carbon at $t = 0$, D_c is the diffusion coefficient of that element in a material, and x is the position of interest. For carbon diffusing in γ -austenite, the diffusion coefficient can be expressed as:

$$D_c = 2.3 \cdot 10^{-5} \exp\left(-\frac{148}{8.314 \cdot T}\right) \quad (2)$$

Where T is the temperature in K and D_c is the diffusion coefficient in m^2s^{-1} . Although Eq. (2) is a fairly accurate model in decarburization studies, it does not take into consideration the scale formed during exposure to elevated temperatures. Such a layer acts as a simultaneous source to the formation of carbon monoxide and a barrier to the removal of it. Equation (2) only represents the diffusion of carbon through γ -austenite by "random jumps," and not the additional barrier of the scale. Such random jumps are dependent on the thermal energy, interstitial sites available, and activation energy of a carbon atom leaving its initial site. The effect of adding a scaling

factor into a decarburization model was proposed by Birks and Jackson (1970) in his research work. It is possible to evaluate the depth of decarburization as the position where the carbon content is 90% of the original carbon content. Equation (3) expresses the depth of decarburization, d_{B-J} , for an austenitic steel at temperature T with no initial decarburization ($d = 0$ for $t = 0$). In addition, it is reported that the values predicted by Eq. (3) are about twice the depth observed in practice for carbon steels annealed in the austenitic range of $900^\circ \leq T \leq 1300^\circ \text{C}$ (Birks and Jackson, 1970; Birks *et al.*, 2006). Therefore, for the comparison with the experimental results of d_{exp} obtained in TWIP steel one half of the predicted value obtained by Eq. (3) has been used.

$$d_{B-J} (\mu\text{m}) = 10^4 \cdot 0.686 \cdot t^{\frac{1}{2}} \cdot \exp\left(-\frac{8140}{T}\right) \quad (3)$$

In Fig. 7 the depth of decarburized layer evaluated metallographically as depth of sub-surface zone with microstructure γ -austenite + α' -martensite, d_{exp} is plotted together with Eq. (3), d_{B-J} (Birks and Jackson, 1970; Birks *et al.*, 2006). As it can be noted the agreement with the experimental results is fairly good from the model calculations.

4.2. Differences in decarburation behavior of TWIP and C45 steels

As it can be remarked, in the range of soaking time explored 300 s – 1100 s, the decarburization depth of TWIP steels is larger than C45 steel. This difference between both steels could be explained

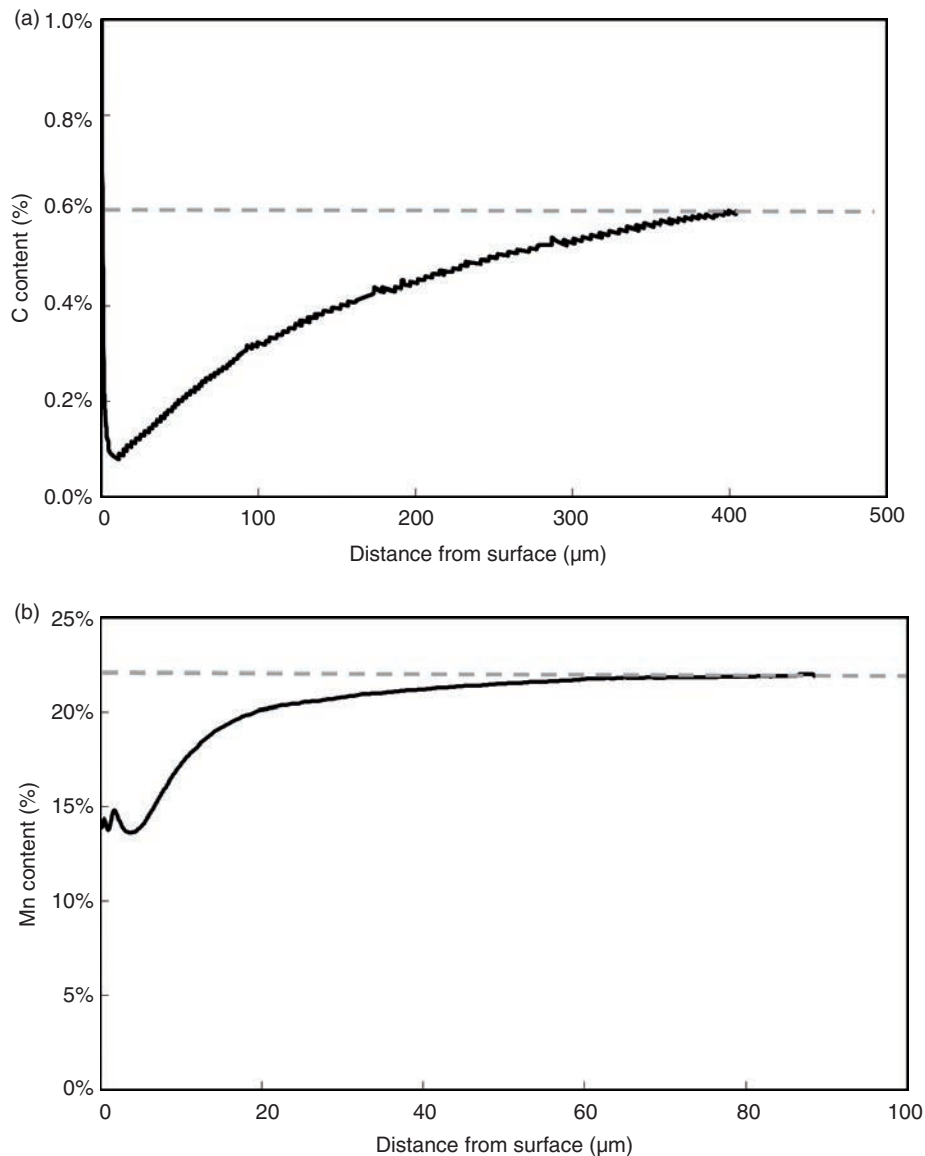


FIGURE 6. GDOES concentration profiles after annealing treatment of 1200 °C - 1100 s for TWIP steel with composition 22% Mn, 0.6% C: (a) C content profile and (b) Mn content profile.

as a dissimilar behavior during the annealing treatments of these steels in the temperature range $T < 910$ °C.

In fact, for the TWIP steels the carbon is in solid solution in the crystal structure and it is ready to react with oxygen even at relatively low temperature. In the case of C45 steel, the amount of decarburization at lower temperature during heating is low due to phase transformation α -Ferrite + Pearlite \rightarrow γ - austenite in the temperature range [750 °C - 910 °C] estimated by means of Thermo-calc (TCFe6 database). During this transient the α -Ferrite layer characterized by low carbon solubility on the strip surface slows down the steel decarburization kinetics. Therefore, in the temperature range [750 °C - 910 °C] the decarburization kinetics of TWIP steel

is faster than that of C45 steel. This fact could explicate the difference in decarburization behavior of both TWIP and C45 steels.

4.3. Hardness in the annealed samples of TWIP steel

Regarding the hardness (HV200 g), for TWIP steel, the outer zone of the sub-surface (γ -austenite + α' -martensite) reveals a quite high hardness values with respect to bulk (γ -austenite), as it can be seen in Table 2. Indeed, the outer zone of the sub-surface is characterized by a higher amount of α' -martensite (low C and Mn content), whereas the presence of α' -martensite is lower towards the bulk, since Mn content approaches the nominal content. This highlights that the ductility of the sub-surface zone is

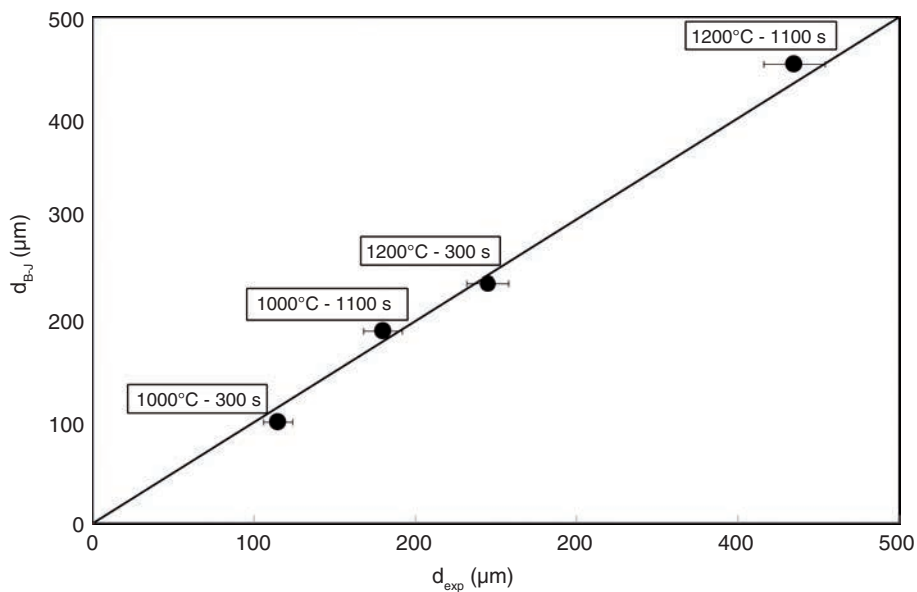


FIGURE 7. Depth of decarburized layer evaluated metallographically, d_{exp} , versus depth of decarburization using Birks-Jackson model, $d_{B,J}$ TWIP steel.

TABLE 2. Hardness Vickers (HV_{200g}) values of TWIP. Bulk and sub-surface zone. Annealing treatments: 1000 °C - 300 s and 1200 °C - 1100 s

Material	1000 °C - 300 s		1200 °C - 1100 s	
	Bulk (HV)	Sub-Surface (HV)	Bulk(HV)	Sub-surface (HV)
TWIP STEEL	*178 ± 10	**265 ± 16	*189 ± 11	**320 ± 14

*IT CORRESPONDS TO γ -austenite phase

** It corresponds to γ -austenite+ α' -martensite phases

quite low with respect to the bulk for the TWIP steel (Ghasri-Khouzani and McDermid, 2015). This microstructural heterogeneity in the sub-surface for TWIP steel affects the ductility of the material in subsequent mechanical tests.

4.4. Effect of decarburation on the SFE in TWIP steel

The *SFE* of a material not only depends on the composition but also on temperature (Grässel *et al.*, 1997; Grässel and Frommeyer, 1998). Allain *et al.* (2004) researched on the Fe-22Mn-0.6 C (% in mass) TWIP steel and they deduced that strain-induced martensitic (ϵ -martensite) transformation (SIMT) occurred for calculated *SFE* of γ -austenite below $18 \text{ mJ}\cdot\text{m}^{-2}$ although, twinning induced plasticity took place in the interval of $12 - 35 \text{ mJ}\cdot\text{m}^{-2}$. Thermodynamic *SFE* calculations performed by Saeed-Akbari *et al.* (2009) pointed out that SIMT is a more likely deformation mechanism until $20 \text{ mJ}\cdot\text{m}^{-2}$. In the bibliography, there is a deficiency of agreement in the *SFE* values calculated via thermodynamic methods, which are associated with deformation mechanisms. It is concluded that the main reason for that comes from different

thermodynamic parameters and interfacial energies $\sigma^{\gamma/\epsilon}$, ranging from $5 \text{ mJ}\cdot\text{m}^{-2}$ to $27 \text{ mJ}\cdot\text{m}^{-2}$ for Fe-Mn-based alloys (Pierce *et al.*, 2014).

In the current case, the presence of α' -martensite in the C and Mn depleted sub-surface zone is due to the local lowering of *SFE* of γ -austenite. Although, there is not experimental data for *SFE* in this work, an alternative approach like embedded-atom method (EAM), can be applied to γ -austenite in Fe-Mn alloys (Rong *et al.*, 2003). The calculated results based on Johnson’s truncation model and its modified model indicates that *SFE* of γ -austenite in Fe-20Mn alloy is in accordance with the thermodynamically calculated one. The *SFE* of γ -austenite at room temperature in Fe-Mn alloys with $20 \leq y \leq 55$ can be expressed as Eq. (4):

$$SFE(\text{m}\cdot\text{J}\cdot\text{m}^{-2}) = 23.3 + 0.269y \tag{4}$$

where y is the chemical composition of Mn (% in mass).

Assuming Eq. (4) in the interval $20 \leq y \leq 22$ for decarburized zone in TWIP steel, the *SFE* of γ -austenite drops as a consequence of the depletion in

Mn. In the decarburized zone in addition to α' -martensite, a less stable γ – austenite is observed prone to undergo *SIMT*. Hence, the microstructural heterogeneity (γ – austenite + α' -martensite + ϵ – martensite) can also contribute to an earlier structural damage during mechanical test.

5. CONCLUSIONS

The main conclusions of this research work concerning the 22% Mn-0.6% (% in mass) TWIP steel are:

- The differences in ductility observed in TWIP steels after annealing at high temperatures are a combination of the intrinsic effect of grain size on strength and work hardening rate and extrinsic effect related to decarburization and Mn depletion producing a mixed of γ – austenite + α' -martensite microstructure in the sub-surface zone during the annealing treatments.
- The loss of ductility in coarse-grained TWIP steel can be attributed to α' -martensite and a less stable γ – austenite with lower *SFE* in the decarburized zone. For 1200 °C - 1100 s the depth of Mn depleted zone (typically < 80 μ m) is significantly lower than C decarburized layer (< 420 μ m).
- The theory derived by Birks and Jackson (1970) allows predicting the thickness of the decarburized layer at temperatures higher than 1000 °C for the soaking times longer than 300 s in TWIP steel.
- The final annealing process after cold rolling can be critical for the industrial production of TWIP steel. A controlled annealing furnace atmosphere has to be considered in order to avoid the occurrence of decarburization and Mn depletion.

ACKNOWLEDGEMENTS

Economical support from the European Union, Research Programme of the Research Fund for Coal and Steel (contract RFSR-CT-00030) and from the Spanish Ministry of Science and Innovation (action MAT2005-23927-E). We would like to thank A. Ferraiuolo, D. Badiola and A. Córcoles for their scientific support in this research work. Finally, I would like to show my deep appreciation to J. de las Cuevas, M. de las Cuevas, P. Jiménez and C. Cardona.

REFERENCES

Allain, S., Chateau, J.P., Bouaziz, O., Migot, S., Guelton, N. (2004). Correlations between the calculated stacking fault energy and the plasticity mechanisms in Fe-Mn-C alloys. *Mater. Sci. Eng. A* 387–389, 158–162. <http://dx.doi.org/10.1016/j.msea.2004.01.059>.

Ankem, S., Greene, C.A., Aiyangar, A.K. (1999). Recent developments in growth kinetics of deformation twins in bulk

metallic materials. *Proceedings of the Symposium. on Adv. in Twinning: The Minerals, Metals & Mater. Society*, pp. 127–143.

Birks, N., Jackson, J. (1970). Quantitative treatment of simultaneous scaling and decarburization of steels. *J. Iron Steel Inst.* 208, 81–85.

Birks, N., Meier, G.H., Pettit, F.S. (2006). *Introduction to the High-temperature Oxidation of Metals*. 2nd Ed., Cambridge University Press, New York.

Bouaziz, O., Allain, S., Scott, C. (2008). Effect of grain and twin boundaries on the hardening mechanisms of twinning-induced plasticity steels. *Scripta Mater.* 58 (6), 484–487. <http://dx.doi.org/10.1016/j.scriptamat.2007.10.050>.

Bouaziz, O., Allain, S., Scott, C.P., Cugy, P., Barbier, D. (2011). High manganese austenitic twinning induced plasticity steels: A review of the microstructure properties relationships. *Curr. Opin. Solid State Mater. Sci.* 15 (4), 141–168. <http://dx.doi.org/10.1016/j.cossms.2011.04.002>.

Chen, L., Zhao, Y., Qin, X. (2013). Some Aspects of High Manganese Twinning-Induced Plasticity (TWIP) Steel, A Review. *Acta Metall. Sin.* 26 (1), 1–15. <http://dx.doi.org/10.1007/s40195-012-0501-x>.

Cornette, D., Cugy, P., Hildenbrand, A., Bouzekri, M., Lovato, G. (2005). Ultra high strength FeMn TWIP steels for automotive safety parts. *Rev. Metall-Paris CIT* 102 (12), 905–918. <http://dx.doi.org/10.1051/metal:2005151>.

De Cooman, B.C., Chin, K.-G., Kim, J.M. (2011). *New Trends and Developments in Automotive System Engineering. High Mn TWIP Steels for Automotive Applications*, Chapter 6, Editor Marcello Chiaberge.

De las Cuevas, F., Reis, M., Ferraiuolo, A., Pratalongo, G., Karjalainen, L.P., Alkorta, J., Gil Sevillano, J. (2010a). Hall-Petch relationship of a TWIP steel. *Key Eng. Mater.* 423, 147–152. <http://dx.doi.org/10.4028/www.scientific.net/KEM.423.147>.

De las Cuevas, F., Reis, M., Ferraiuolo, A., Pratalongo, G., Karjalainen, L.P., Garcia Navas, V., Gil Sevillano, J. (2010b). Kinetics of recrystallization and grain growth of cold rolled TWIP steel. *Adv. Mater. Res.* 89–91, 153–158. <http://dx.doi.org/10.4028/www.scientific.net/AMR.89-91.153>.

De las Cuevas, F., Ferraiuolo, A., Karjalainen, L.P., Gil Sevillano, J. (2014). Propiedades mecánicas a tracción de un acero TWIP a altas velocidades de deformación: relación de Hall-Petch. *Rev. Metal.* 50 (4), e031. <http://dx.doi.org/10.3989/revmetalm.031>.

Fick, A. (1855). Ueber Diffusion. *Ann. Physik-Leipzig* 170 (1), 59–86. <http://dx.doi.org/10.1002/andp.18551700105>.

Frommeyer, G., Grässel, O. (1998). Light Constructional Steel and the Use Thereof. Patent PCT/EP98/04044. WO 99/01585 A1.

Frommeyer, G., Drewes, E.J., Engl, B. (2000). Physical and mechanical properties of iron-aluminium-(Mn, Si) light-weight steels. *Rev. Metall-Paris* 97 (10), 1245–1253. <http://dx.doi.org/10.1051/metal:2000110>.

Galán, J., Samek, L., Verleysen, P., Verbeken, K., Houbaert, Y. (2012). Advanced high strength steels for automotive industry. *Rev. Metal.* 48 (2), 118–131. <http://dx.doi.org/10.3989/revmetalm.1158>.

Ghasri-Khouzani, M., McDermid, J.R. (2015). Effect of carbon content on the mechanical properties and microstructural evolution of Fe-22Mn-C steels. *Mater. Sci. Eng. A* 621, 118–127. <http://dx.doi.org/10.1016/j.msea.2014.10.042>.

Grässel, O., Frommeyer, G. (1998). Effect of martensitic phase transformation and deformation twinning on mechanical properties of Fe-Mn-Si-Al steels. *Mater. Sci. Tech.* 14 (12), 1213–1217. <http://dx.doi.org/10.1179/mst.1998.14.12.1213>.

Grässel, O., Frommeyer, G., Derder, D., Hofmann, H. (1997). Phase transformation and mechanical properties of Fe-Mn-Si-Al TRIP-steels. *J. Phys. IV France* 7, - C5.383-C5.388. <http://dx.doi.org/10.1051/jp4:1997560>.

Grässel, O., Krüger, L., Frommeyer, G., Meyer, L.W. (2000). High strength Fe-Mn-(Al, Si) TRIP/TWIP steels development - properties - application. *Int. J. Plasticity* 16 (10–11), 1391–1409. [http://dx.doi.org/10.1016/S0749-6419\(00\)00015-2](http://dx.doi.org/10.1016/S0749-6419(00)00015-2).

Gil Sevillano, J., de las Cuevas, F. (2012). Internal stresses and the mechanism of work hardening in twinning-induced

- plasticity steels. *Scripta Mater.* 66 (12), 978–981. <http://dx.doi.org/10.1016/j.scriptamat.2012.02.019>.
- Goldberg, A., Ruano, O.A., Sherby, O.D. (1992). Development of ultrafine microstructures and superplasticity in Hadfield manganese steels. *Mater. Sci. Eng. A* 150 (2), 187–194. [http://dx.doi.org/10.1016/0921-5093\(92\)90111-D](http://dx.doi.org/10.1016/0921-5093(92)90111-D).
- Hadfield, R.A. (1883). High manganese steel. British Patent N° 200/1883.
- Khalissi, M., Singh Raman, R.K., Khoddam, S. (2011). Stress Corrosion Cracking of Novel Steel for Automotive Applications. *Procedia Eng.* 10, 3381–3386. [http://dx.doi.org/10.1016/0921-5093\(92\)90111-D10.1016/j.proeng.2011.04.557](http://dx.doi.org/10.1016/0921-5093(92)90111-D10.1016/j.proeng.2011.04.557).
- Koyama, M., Sawaguchi, T., Tsuzaki, K. (2012a). Quasi-cleavage Fracture along Annealing Twin Boundaries in a Fe–Mn–C Austenitic Steel. *ISIJ Int.* 52 (1), 161–163. <http://doi.org/10.2355/isijinternational.52.161>.
- Koyama, M., Akiyama, E., Tsuzaki, K. (2012b). Hydrogen embrittlement in a Fe–Mn–C ternary twinning induced plasticity. *Corros. Sci.* 54, 1–4. <http://dx.doi.org/10.1016/j.corsci.2011.09.022>.
- Lin, H.C., Lin, K.M., Lin, C.S., Ouyang, T.M. (2002). The corrosion behavior of Fe-based shape memory alloys. *Corros. Sci.* 44 (9), 2013–2026. [http://dx.doi.org/10.1016/S0010-938X\(02\)00027-6](http://dx.doi.org/10.1016/S0010-938X(02)00027-6).
- Pierce, D.T., Jiménez, J.A., Bentley, J., Raabe, D., Oskay, C., Witting, J.E. (2014). The influence of manganese content on the stacking fault and austenite / ϵ -martensite interfacial energies in Fe–Mn–(Al–Si) steels investigated by experiment and theory. *Acta Mater.* 68, 238–253. <http://dx.doi.org/10.1016/j.actamat.2014.01.001>.
- Pierce, D.T., Jiménez, J.A., Bentley, J., Raabe, D., Oskay, C., Witting, J.E. (2015). The influence of stacking fault energy on the microstructural and strain hardening evolution of Fe–Mn–Al–Si steels during tensile deformation. *Acta Mater.* 100, 178–190. <http://dx.doi.org/10.1016/j.actamat.2015.08.030>.
- Rong, Y.H., Meng, Q.P., He, G., Xu, Z.Y. (2003). Calculation of the Stacking Fault Energies of Fe–Mn Alloys by Embedded-Atom Method. *Journal Shanghai Jiaotong University* 37, 171–174. http://en.cnki.com.cn/Journal_en/C-C000-SHJT-2003-02.htm.
- Saeed-Akbari, A., Imalau, J., Prah, U., Bleck, W. (2009). Derivation and Variation in Composition-Dependent Stacking Fault Energy Maps Based on Subregular Solution Model in High-Manganese Steels. *Metall. Mater. Trans. A* 40 (13), 3076–3090. <http://dx.doi.org/10.1007/s11661-009-0050-8>.
- Scott, C., Allain, S., Faral, M., Guelton, N. (2006). The development of a new Fe–Mn–C austenitic steel for automotive applications. *Rev. Metall-Paris* 103 (6), 293–302. <https://dx.doi.org/10.1051/metal:2006142>.
- Sipos, K., Remy, L., Pineau, A. (1976). Influence of austenite predeformation on mechanical properties and strain-induced martensitic transformations of a high manganese steel. *Metall. Trans. A* 7 (5), 857–864. <https://dx.doi.org/10.1007/BF02644083>.
- Tomota, Y., Strum, M., Morris, J.W. (1987). The relationship between toughness and microstructure in Fe–high Mn binary alloys. *Metall. Mater. Trans. A* 18 (6), 1073–1081. <https://dx.doi.org/10.1007/BF02668556>.